Renewable Energy 222 (2024) 119857

Contents lists available at ScienceDirect

Renewable Energy

journal homepage: www.elsevier.com/locate/renene

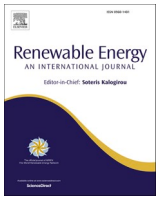

A novel approach for incidence angle modifier calculation of arbitrarily oriented linear Fresnel collectors: Theory, simulations and case studies

Samuele Memme, Marco Fossa *

DIME - Department of Mechanical, Energy, Management and Transportation Engineering, University of Genova, Italy

ARTICLE INFO

Keywords:
Concentration solar plants
Linear Fresnel collector orientation
Optical and energy efficiency
Raytracing simulations
Fresnel plant optimization
Incidence angle modifier

ABSTRACT

The easiest possibility to assess the combined opto-energy efficiency of Linear Fresnel Collectors (LFC) is to refer to the Incidence Angle Modifier (IAM) concept: for this kind of solar collector, IAM calculation is often performed according to the so-called factorization method. Unfortunately, the factored IAM fails in providing reliable results of the real LFC yield. In this investigation, hourly 3D ray tracing simulations have been carried out on two case-study plants located in Morocco and Italy: reference ray tracing calculated IAMs have been used to develop simple correlations for inferring the instantaneous IAM of arbitrarily aligned LFCs. Instantaneous IAM formulas resulted to be able to provide yield predictions with a Root Mean Square Error equal to 5.57 % of the yearly average IAM, much lower than the factorization method (19.42 %). Subsequently, a reduced 3-day dataset of ray tracing values has been considered to calibrate the regression constants, resulting in still high accuracy for orientations not exceeding 30°. Finally, the analysis of available power at the receiver allowed to further assess the robustness of the proposed approach regardless of the plant orientation angles.

1. Introduction

Renewable energy exploitation has become a crucial aspect within the actions for mitigating climate change: by the end of 2021, renewables accounted for 38 % of installed global capacity [1], thanks to lower investment costs with respect to the past and institutional incentives. The European Union has promoted the deployment of renewable energy sources through initiatives as the well-known "Fit for 55" on its path to carbon neutrality; on the other hand, the "RepowerEU" strategy is aimed at exploiting the full potential of the European Union power sector through increased investment in renewable energy and energy efficiency, while the "Next Generation EU" supports investments by means of financial aids towards renewable energy goals. In this context, renewable energy, with a focus on solar thermal energy, plays a crucial role in increasing the efficiency of energy production systems and the share of distributed generation plants: Concentrated solar power (CSP) global installed capacity increased from 2567 MW (2012) to 6387 MW (2021) [1], although relatively high investment costs, as well as limited support to fully unlock storage capabilities, are supposed to limit the new installed capacity just by 5 GW in the period 2022–2027 [2]. Some regions of the world have particularly favourable climatic conditions for the operation of solar thermal plants. In these locations, the levelized cost of electricity (LCOE) from CSP plants can compete with that of fossil fuel power plants. In addition, solar thermal power generation mitigates some of the limitations that affect the photovoltaic and wind systems in terms of intermittency and the need for electrical energy storage: the integration of CSP plants with thermal energy storage (TS) systems, in fact, is an effective solution for peak shaving and load levelling [3], able to induce a 68 % reduction [4] in the weighted LCOE of solar thermal energy from 2010 to 2021. In terms of installed capacity, there are currently 6 GW of operational CSP plants worldwide, according to a report by the World Bank [5], most of which are concentrated in Spain (2.3 GW), the U.S.A. (1.6 GW), Morocco (0.53 GW), China (0.5 GW), and South Africa (0.5 GW).

Two main CSP technologies can be distinguished: point-focusing and line-focusing, with the latter accounting for about 81 % of the current global capacity [6]. Among the available line-focusing CSP technologies, Linear Fresnel Collectors (LFC) have a promising potential and several notable real-world applications as a thermal energy source alternative to traditional fossil fuels for industrial processes where fluid temperatures below 400 °C are required [7,8]: similar to the more diffused linear Parabolic Trough (PT) collectors, LFC differs in the fact that the mirror concentrator is divided into a number of horizontally arranged linear and flat, or slightly elastically curved, primary mirrors. Sun rays are then reflected onto an absorber tube, which is in turn housed in a secondary

* Corresponding author.
E-mail address: marco.fossa@unige.it (M. Fossa).

https://doi.org/10.1016/j.renene.2023.119857
Received 20 June 2023; Received in revised form 15 December 2023; Accepted 16 December 2023
Available online 21 December 2023

Nomenclature

Symbols

DNI	Direct normal irradiance [W/m^2]
E	Solar irradiance [W/m^2]
F	Factored approximation
g	Gap, horizontal spacing between adjacent mirrors [m]
H	Height of the receiver assembly [m]
L_m	Length of the primary mirror row [m]
N_m	Number of mirror rows
$\vec{N}$	Vector perpendicular to the mirror surface
Nday	Day number
$\vec{R}$	Vector representing reflected ray direction
r_m	Mirrors radius of curvature [m]
$\vec{S}$	Vector pointing sun position
W_{CPC}	Transversal width of secondary receiver cavity [m]
W_m	Width of the single primary mirror [m]

Greek letters

α	Primary mirrors absorptivity [−]
α_s	Solar altitude angle [°]
α_p	Profile angle [°]
β	Tilt angle of primary mirrors [°]
γ_s	Solar azimuth angle [°]
δ	Solar declination angle [°]
ζ	Primary mirror orientation as measured from north to south direction [°]
η	Opto-energy efficiency of a Linear Fresnel plant
θ_L	Longitudinal component of solar zenith angle [°]
θ_s	Solar zenith angle [°]
θ_T	Transversal component of solar zenith angle [°]
θ_w	Incidence angle [°]
λ_{surf}	Angular deviation of the reflected vector [mrad]
ρ	Primary mirrors reflectivity [−]
σ_{te}	Angular deviation of the tracking system [mrad]
τ	Primary mirrors transmissivity [−]
φ	Latitude [°]

Subscripts

d	Daily average
e	Electric
j	Mirror row number
m	Mirror
r	Sun ray
rel	Relative
s	Sun
y	Yearly average

Acronyms

CPC	Compound parabolic collector
CSP	Concentrating solar power
EW	East-west orientation
GHG	Greenhouse gases
IAM	Incidence angle modifier
LCOE	Levelized cost of electricity
LFC	Linear Fresnel collector
MCRT	Monte Carlo ray tracing
NS	North-south orientation
P1	Plant 1, Partanna (Italy) case study
P2	Plant 2, Green Energy Park (Morocco) case study
PT	Parabolic trough
PV	Photovoltaic
RT	Ray tracing
TS	Thermal energy storage
ZP	Zenith projections

concentrator, usually in the shape of a trapezoidal cavity or a compound parabolic collector (CPC), i.e., a non-imaging concentrator with a low concentrating ratio (1–5) [9,10]. Advantages of this solution include the low wind load to which LFCs are subject [11], which allows them to be cost-effective [12] and suitable for installation both on remote areas and flat roofs within urban scenarios [12–14], despite the intrinsic lower optical efficiency, if compared to that of PT [15–17]. Additionally, it should be highlighted the lower required land use with respect to other CSP technologies, which has been quantified by Cau and Cocco [18] in about 55–60 kWh$_e$/y/m^2 for LFC with respect to 45–50 kWh$_e$/y/m^2 for PT, thanks to concentration ratio which usually ranges between 30 and 80 compared to 80–90 of PT [19]. Finally, Wang et al. [20] demonstrated that LFC outperforms other available CSP solutions in terms of concentrating uniformity, thus allowing fewer mechanical stresses on the receiving absorber, promoting LFC as a proper solution also for PV applications [21].

Optical design optimization of LFs is a topic of particular interest to reduce the negative effects of shadows on collector performance: analyses of design elements to this aim include the number and width of mirrors, the height of the receiver, the shape of its reflector, the distance between mirrors and the orientation of the plant. The effect of mirrors spacing has been studied by many authors: Abbas et al. [22] compared it against the effect of variable width, while the number of mirrors and their gap have been used as variable parameters by Singh et al. [23]; mirrors' curvature is another key parameter to design reflectors with the proper focal distance, as highlighted by several research works [24–27]. Another variable that can severely affect the amount of collectible energy from a generic solar system is the orientation of the plant: non-tracking solar applications in the northern hemisphere can achieve their optimal configuration when installed facing south according to a tilt angle to be determined taking into account average local weather conditions, as discussed for example in Ref. [28] by Memme and Fossa. Regarding LFC orientation ζ, i.e., the azimuth angle of the longitudinal axis of the system with respect to the north-south direction, it should be noted that these plants are usually aligned along the north-south (NS) direction because this increases overall optical performance [29] and reduces the variation of energy delivery along the day [30]. Most research works assume this mentioned "standard" orientation, thus neglecting the effects of this parameter in terms of optical losses. On the other hand, east-west oriented installations allow for more constant energy production on a yearly basis [15,31,32]. Some published works considered the effect of LFC orientation on its optical efficiency: Huang et al. [33] proposed an LFC equipped with a solar azimuth tracking system, assessing its performance by ray tracing analysis, while an analytical approach has been proposed by Sharma et al. [34] to evaluate different optical losses under variable orientations. A real facility has been studied by Montanet et al. [35] in the frame of a comprehensive topography analysis of a plant located in France.

As mentioned earlier, ray tracing analysis demonstrates robustness and generates results of high precision and accuracy. Conversely, conducting year-long hourly analyses necessitates extensive post-processing of multiple data sets, thereby significantly augmenting the computation time required. To alleviate the computational workload, especially when energy estimations are a part of parametric economic analyses, the optical performance can be performed using a metric known as the Incidence Angle Modifier (IAM), which quantifies the ratio between the optical efficiency at a generic sun position and the optical efficiency under normal incidence [36]. While for collectors which are

symmetrical about the collector normal IAM can be expressed by means of a polynomial equation [37], non-imaging collectors, including LFC, need a complex function to describe their IAM with a sufficient degree of accuracy [38]. Very often a suggested approach is the factorization method, as proposed by McIntire [39]: according to this model, the solar mirror performance at any possible sun position in the sky is estimated as the product of the longitudinal and transversal IAM.

This work aims to identify and present a new alternative correlation for IAM, based on properly selected independent variables that can successfully describe the performance of arbitrarily oriented LF systems, evaluating their accuracy with respect to the well-known factored approach introduced by McIntire [39]. Following a similar approach to the one proposed by Boccalatte et al. [19], in which a IAM correlation is proposed for just the north-south (NS) orientation as a function of solar zenith and declination angle, herein a more comprehensive correlation is performed: the problem of arbitrarily oriented LFCs is tackled, starting from the analysis of existing LFC plants in the Mediterranean area. In details, two reference geometries have been considered, namely the one of the plant in Partanna (Italy) and the one related to the facility in Ben Guerir (Morocco), both characterized by axis azimuth different from 0°. By means of 3D ray-tracing simulations carried out using the FresnelSim code developed by the present research group [40,41], an "exact" dataset of IAM has been obtained, which has then been used to assess the accuracy of the considered approximating formulas. These include the factorization correlation by McIntire [39], whose results are affected by non-negligible errors due to the factorization of non-factorable phenomena, and a new polynomial correlation, defined as a function of the longitudinal and transversal projections of the zenith angle. The present approach and related formulas show a higher accuracy when the set of polynomial coefficients is calculated for the specific plant orientation, but it has been demonstrated that a single set of coefficients can fit all the possible orientations in the range of 0°–90° with a sufficiently low RMSE. The possibility to reduce the needed ray tracing dataset to calibrate the regression constants is explored as well, while, in the final part of the analysis, results are critically presented in the form of power available at the secondary receiver, thus assessing the strengths and weaknesses of both correlations.

2. Modeling and methodology

2.1. FresnelSim algorithm

FresnelSim is a simulation tool devoted to Monte-Carlo ray-tracing (MCRT) analysis aimed at characterizing LFC performance based on a series of efficiency indicators [40]. Its algorithm has been defined in Matlab environment by the present research group and the underlying mathematical model has been presented and verified against Tonatiuh [42], a well-known open-source ray tracing software for solar applications. FresnelSim can be distinguished by the available codes and software (e.g. Soltrace [43], TieSOL [44], OTSun [45], TracePro [46], spbRAY [47]) in that it has been specifically designed for LFC: in particular, it's easy to modify the geometric parameters of the primary mirror field and the secondary receiver, even for those who don't have an in-depth knowledge of the plant geometry and optical phenomena. The user can specify a set of parameters including mirror dimensions, curvatures, spacing between them, receiver height, geometric characteristics of the CPC, and a series of optical characteristics such as mirror reflectivity, receiver tube absorptivity, mirror tracking system error and angular deviation of the reflected ray. Additional simulation variables concern the time horizon on which to carry out the calculations: this allows to perform instantaneous, daily or annual fast simulations of how the primary design parameters impact the system's optical-energy efficiency. The simulation results are consistently presented in a comprehensive summary, encompassing various optical and energy efficiencies of the system: the user has the option to choose whether the calculations are based on the primary mirror area, or the overall surface area occupied by the system. Furthermore, efficiency can be evaluated by considering the energy reaching the aperture of the CPC collector or directly to the vacuum tube: the calculation is performed assuming the sun as a point source, whose position is uniquely defined by the solar azimuth γ_s and elevation angles α_s, introduced in the following section. Additionally, it is feasible to assess individual optical losses independently, thereby considering the impact of different mirror field arrangements on shading, blocking, end-losses, and cosine efficiency individually. A recent enhancement of the FresnelSim algorithm enables the simulation of plant configurations that deviate from the standard NS orientation: this eliminates the need for users to utilize relative, rotated reference systems to define the geometry of the plant, thus accounting for a comprehensive range of practical cases, in which space constraints often lead to non-optimal orientations.

For the purposes of this study, the efficiency indicator considered for performance analysis is defined as the ratio of the energy concentrated onto the aperture area of the secondary receiver to the net energy on the primary mirrors field, according to Eq. (1).

$$\eta_{opt,en} = \frac{\sum_{n=1}^{N_{Ap_{CPC}}} E_{r,j}}{DNI \bullet [N_m \bullet L_m \bullet (W_m + g) - g \bullet L_m]} \tag{1}$$

In detail, DNI is the time-varying direct normal irradiance derived from the clear sky model proposed by Duffie and Beckman [48] in W/m^2, while N_m is the total number of primary mirrors; all the geometric parameters are defined according to Fig. 1, while $E_{r,j}$ (Eq. (2)) is the power associated to the single ray impinging on the jth mirror, whose incidence angle is $\theta_{w,j}$, according to its own tilt angle β_j.

$$E_{r,j} = \frac{DNI \bullet L_m \bullet W_m \bullet \cos(\theta_{w,j})}{N_{rays}} \tag{2}$$

2.2. Ray-tracing model for arbitrarily oriented LFC

The general working principle of the FresnelSim algorithm has been detailed by the present research group in a dedicated research paper [40], to which the reader is addressed for more in-depth information. In summary, a user-defined number of rays are initialized on each primary mirror of a specified LFC geometry. After conducting checks to determine whether the ray is affected by mirror-by-mirror phenomena, i.e., shading or blocking, or by CPC receiver shadow, each ray is associated with a vector $\vec{R}$ representing its direction after reflection. This vector is determined using the well-known Snell-Descartes law, taking as inputs

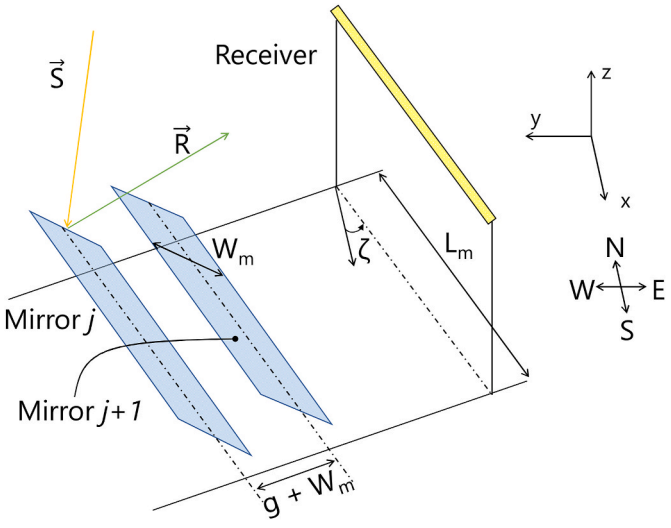

Fig. 1. Schematic representation of a LFC, including the definition of a series of geometrical parameters employed in the present investigation [41].

the vectors $\vec{S}$, pointing towards the current position of the Sun, and $\vec{N}$, representing the normal direction relative to the mirror plane. The intersection of $\vec{R}$ with a horizontal plane at the height of the secondary concentrator allows to determine whether the solar ray and its energy content are intercepted by the secondary concentrator or lost, i.e., due to spillage and end losses.

In order to assess the influence of the plant azimuth orientation on the optical and energy performance of a LFC, the original FresnelSim algorithm has been recently improved to account for orientations other than the optimal NS direction, as presented by Memme and Fossa in Ref. [41]. To this aim, the concept of the "apparent" relative solar azimuth was introduced (Eq. (3)). This is defined as the solar azimuth angle minus the system's orientation azimuth angle. Herein, the orientation is indicated by the clockwise deviation from the north-south direction of a system that is rotated on the ground plane around the vertical axis passing through the midpoint of its axis of symmetry (Fig. 1).

$$\gamma_{rel} = \gamma_s - \zeta \tag{3}$$

Based on this assumption, the relative position of the sun $\vec{S}_{rel}$ (Eq. (4)) can be accurately described by appropriately adjusting the sun vector using the following equation. It should be specified that, according to Figs. 1 and 2, the x axis represents the north-south direction and is positive towards south, while the perpendicular y axis points towards west.

$$\vec{S}_{rel} = \left[S_{x,rel}, S_{y,rel}, S_z\right] = \left[\cos(\alpha_s) \bullet \cos(\gamma_{rel}), \cos(\alpha_s) \bullet \sin(\gamma_{rel}), \sin(\alpha_s)\right] \tag{4}$$

Solar angles (Fig. 2) are calculated using equations presented in Ref. [48] by Duffie and Beckman: in particular, solar elevation α_s, which represents the angular position of the sun above the horizon, is determined according to Eq. (5), while solar azimuth γ_s, i.e., the horizontal angle with respect to south, is defined in Eq. (6). The complement of the elevation angle is the solar zenith angle θ_s. The following equations, in turn, rely on the latitude φ, solar hour angle ω and declination angle δ, which is determined using the widely known Cooper formula or an equivalent one; the declination angle is assumed to remain constant throughout the day.

$$\alpha_s = \sin^{-1}[\cos(\delta) \bullet \cos(\omega) \bullet \cos(\varphi) + \sin(\delta) \bullet \sin(\varphi)] \tag{5}$$

$$\gamma_s = \sin^{-1}\left[\frac{\cos(\delta) \bullet \sin(\omega)}{\cos(\alpha_s)}\right] \tag{6}$$

FresnelSim also offers a graphical output aimed at providing a readily comprehensible overview of the primary mechanisms that contribute to the efficiency loss of the system: this qualitative analysis proves especially valuable for guiding design decisions aimed at modifying one or more geometric parameters. In this regard, Fig. 3 illustrates a visual representation of the instantaneous simulation of LFC: sun rays correctly reflected onto the designated target are depicted in red, while those appearing in green represent rays reflected outside of the receiver; rays affected by blocking or shading are shown in grey, and those shaded by the CPC are depicted in black.

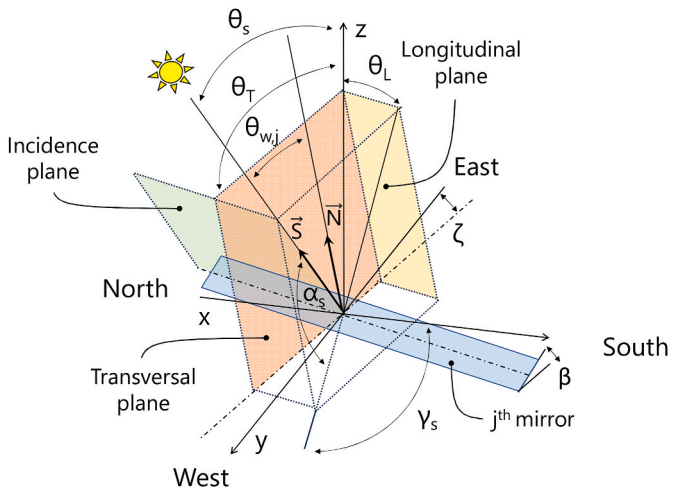

Fig. 2. Schematic representation of solar angles and axis orientation.

2.3. Incidence angle modifier of a linear Fresnel collector

In addition to efficiency indicators defined on a case-by-case basis, the performance of a LFC system in relation to the sun's position can be described through the so-called Incidence Angle Modifier (IAM). As a general definition, the IAM of a solar collector indicates the variation in opto-energy efficiency with the solar incidence angle θ_w, which in turn is the angle between the vector pointing towards the sun and the normal to the aperture plane of the collector itself (Fig. 2). This variation is expressed through an equation in relation to a specific reference solar angle, which is defined based on the collector type and application (Eq. (7)). For LFC application, the IAM is defined as the ratio of the instantaneous opto-energy efficiency, corresponding to a certain position of the sun, to the efficiency value when the sun is at zenith ($\alpha_s = 90°$, $\gamma_s = 0°$).

$$IAM = \frac{\eta_{opt,en}(\theta_w)}{\eta_{opt,en}(\theta_{w,ref})} \tag{7}$$

While a PT concentrator, due to its geometry, just has a longitudinal IAM, LFC have mirrors rows characterized by different tilt angles, so their apertures aren't usually perpendicular to sun rays [49]. Due to the fact that precise IAM calculations based on efficiency results could be obtained by means of time-consuming ray tracing simulations or direct measurements, the factored approach proposed by McIntire [39] is often adopted (Eq. (8)).

$$IAM_F(\theta_T, \theta_L) = IAM_T(\theta_T, 0) \bullet IAM_L(0, \theta_L) \tag{8}$$

In the case of LFC, the biaxial behaviour of the collector requires the specification of longitudinal and transversal angle modifiers, as for all the non-imaging collectors whose optical efficiency is not symmetrical about the collector normal. The latter are defined according to Eqs. (9) and (10) as functions of the transversal and longitudinal components of the solar zenith angle (θ_T and θ_L, Fig. 2), as indicated by Pujol Nadal and Martínez Moll in Ref. [50].

$$IAM_T(\theta_T, 0) = \frac{\eta_{opt,en}(\theta_T, \theta_L = 0°)}{\eta_{opt,en}(\theta_T = 0°, \theta_L = 0°)} \tag{9}$$

$$IAM_L(0, \theta_L) = \frac{\eta_{opt,en}(\theta_T = 0°, \theta_L)}{\eta_{opt,en}(\theta_T = 0°, \theta_L = 0°)} \tag{10}$$

The calculation of the IAM using the biaxial approximation is an accepted practice, although it introduces errors due to the factoring of non-factorable phenomena, such as cosine losses [37]. The factored IAM assumes, at a specific incidence angle, a value given by the product of the corresponding transverse and longitudinal IAMs. In this way, only a reduced set of incidence angles is needed along the two transversal and longitudinal planes, while the IAM is estimated by multiplying the corresponding transversal and longitudinal values.

2.4. Modelling real LFC: the Partanna and Green Energy Park plants

To extend this paper's results to a general context, two specific cases pertaining to currently operational LFC plants have been selected for efficiency and IAM calculations. Considering the availability of geometric details and measurements obtained from bibliographic sources or on-site measurements, the two chosen plants are the ones located in Partanna, Italy, and Ben Guerir, Morocco, which are characterized, as

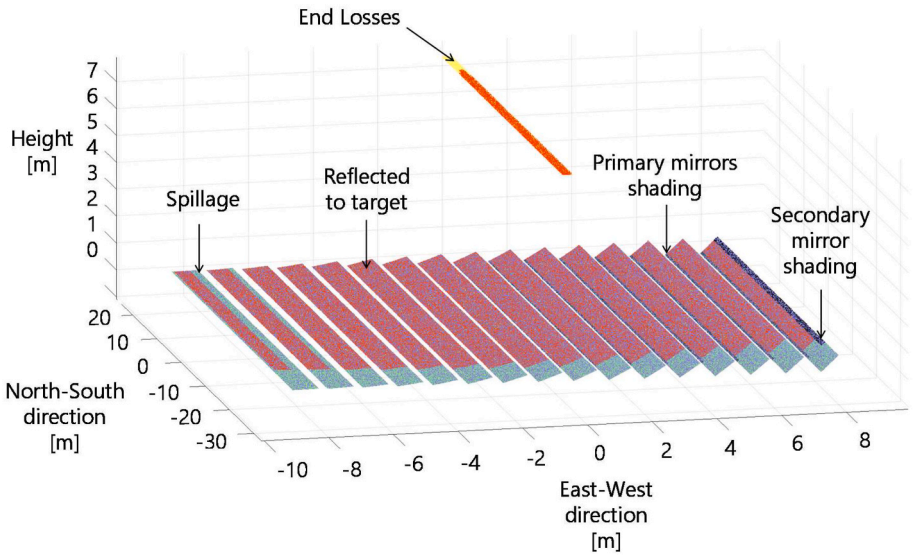

Fig. 3. FresnelSim graphic output for an instantaneous simulation [41].

specified in the following, by different arrangements and orientations.

The Partanna solar power plant (37.70° N, 12.86° E), designed by German company Frenell [51], includes a 5.6 MW_e PV installation and a 4.26 MW_e Linear Fresnel section (Fig. 4) covering an area of about 83200 m^2 [52], with an azimuth orientation angle of about 26° [41]. The primary mirror field is made up of 16 mirror rows arranged in 9 U-shaped loops, each of which consisting of 14 collectors in series, i.e., 800 m in length, corresponding to a 400 m^2 gross mirror area; concerning the secondary reflector, a CPC surrounds the absorber, which operates with molten salts. To extend the energy production timeframe by storing thermal energy for up to 15 h, the plant is equipped with a direct 2-tank thermal energy storage system, based on a "Cold Tank", in which the fluid temperature is about 290 °C, and a "Hot Tank", characterized by fluid temperatures as high as 545 °C; the two tanks are in turn connected to a steam generator for electricity production [53]. The plant entered its production phase, being synchronized with the national high-voltage grid for the first time, in July 2021 [54].

The second case study plant is the LFC at the Green Energy Park (GEP) in Ben Guerir, Morocco (32.2359° N, 7.9538° W), developed by the Research Institute of Solar Energy and New Energies (IRESEN) in collaboration with the Moroccan Ministry of Energy and the OCP Group [55,56]. The plant, whose angle of orientation is 15° with respect to the NS direction, has a total capacity of 1 MW_e and spans a combined aperture area of 16400 m^2, which is divided into two solar fields: 70 % of the gross area is devoted to supplying the organic Rankine cycle (ORC) turbine according to solar irradiance availability, while the remaining 30 % is covered by a solar field whose aim is to charge the TES unit [56]. The mirror field consists of ten rows of slightly curved mirrors, whose total area is equal to 11400 m^2, while the secondary reflector is equipped with a CPC. The plant operates with Delcoterm Solar E15, a thermal oil by Italian D.E.L.CO. Srl [57], whose temperature range is 180 °C–300 °C.

In the following, Table 1 summarizes a set of measurements, estimation reference to existing literature and kind information provided by ENEA research center and IRESEN related to the two reference plants. In general, the precise determination of these parameters is crucial for the performance analysis and optimization of the plant, as well as for the comparison with other solar thermal technologies.

Fig. 4. Bird view of the two reference plants: Partanna CSP plant (P1) on the left and Green Energy Park, Ben Guerir (P2) on the right [58].

2.5. The present model for IAM calculation

The objective of this research is to provide an alternative to time-consuming ray tracing analysis in the form of an analytical equation, which can ensure a higher accuracy compared to the solutions available in literature, particularly with respect to the factored approach proposed by McIntire [39]. To this aim, the instantaneous efficiency of two plants, which constitute the case studies of this work, was determined through FresnelSim. The exact IAM, according to Eq. (7), was calculated with a timestep of 15 min for a total of 25 days equally distributed throughout the year. This set of results was then used to identify the correct set of independent variables to express the IAM trend analytically. While a similar problem has been addressed by the same research group for NS-oriented mirror fields in a recent study [19], in this case, it was chosen to investigate different plant azimuth orientations, from 0° to 90° with a step of 5°. Additionally, to increase the results' general

Table 1
Geometric and optical parameters of the two reference LFC plants.

	Partanna P1	Ben Guerir P2
L_m [m]	400 [53]	12.34 [53]
ζ [°]	26 NW [53]	15 NW
N_m [−]	16 [53]	10 [56]
W_m [m]	0.80 [58,59]	0.63 [40]
H [m]	7.5	4
g [m]	0.28 [58,59]	0.20 [40]
r_m [m]	24 [51]	9.05 [40]
W_{CPC} [m]	0.32 [40]	
σ_{te} [mrad]	1 [11]	
λ_{surf} [mrad]	2 [60–62]	
α [−]	0.06 [40]	
τ [−]	0.00 [40]	
ρ [−]	0.94 [40]	

applicability, the analysis is performed on two different plants with rather different geometries, as they differ both in the number of primary mirrors and in the aspect ratios among their various dimensions.

To identify the most appropriate independent variables, the daily variation of the IAM with respect to a series of solar angles was analysed. While the declination angle is a useful parameter for expressing the daily variation of efficiency indicators during different days of the year for a NS oriented plant, in the present case study, characterized by different orientations, its effectiveness revealed to be limited. Moreover, an intrinsic limitation of this angle is that it does not provide any information regarding the hourly variation of the IAM.

As the mentioned solar angles, although able to describe hourly variations, have limited effectiveness when considering different orientations, it was chosen to consider angles that include information about the orientation of the system itself. In particular, the relative azimuth and the two longitudinal and transversal components of the solar zenith angle θ_s were defined for this purpose based on the angle γ_{rel}, as defined in the previous section (Eq. (3)). In detail, it was found that the two longitudinal and transversal angles express a type of correlation with the IAM that does not change significantly with the orientation of the system. These two angles can be defined starting from the vector product of the z unit vector and the projection of the sun position in the two x and y directions: those projected vectors are defined according to Eq. (11) and Eq. (12), while the longitudinal (θ_L) and transversal (θ_T) zenith angles are expressed in Eq. (13) and Eq. (14).

$$\vec{S}_{rel,T} = \frac{[S_{x,rel}, 0, S_z]}{\|[S_{x,rel}, 0, S_z]\|} = \frac{[\cos(\alpha_s) \bullet \cos(\gamma_{rel}), 0, \sin(\alpha_s)]}{\|[\cos(\alpha_s) \bullet \cos(\gamma_{rel}), 0, \sin(\alpha_s)]\|} \tag{11}$$

$$\vec{S}_{rel,L} = \frac{[0, S_{y,rel}, S_z]}{\|[0, S_{y,rel}, S_z]\|} = \frac{[0, \cos(\alpha_s) \bullet \sin(\gamma_{rel}), \sin(\alpha_s)]}{\|[0, \cos(\alpha_s) \bullet \sin(\gamma_{rel}), \sin(\alpha_s)]\|} \tag{12}$$

$$\theta_L = \cos^{-1}\left[\vec{S}_{rel,L} \bullet (0,0,1)\right] \tag{13}$$

$$\theta_T = \cos^{-1}\left[\vec{S}_{rel,T} \bullet (0,0,1)\right] \tag{14}$$

The next step was to identify the most appropriate trigonometric functions through which to use the two mentioned angles. Through trial and error, it was concluded that the two independent variables should be both expressed in the form of their cosine, namely cos (θ_L) and cos (θ_T). Finally, using the curve fitting tool CurveExpert Professional, v.2.6.5, the cubic (3rd order) polynomial linear regression ended up giving the best results: in the following, this new proposed correlation is indicated as the zenith projections IAM approximation (IAM_{ZP}), defined according to Eq. (15).

$$\begin{aligned} IAM_{ZP} = {} & a + b \bullet \cos(\theta_L) + c \bullet \cos(\theta_T) + d \bullet [\cos(\theta_L)]^2 + e \bullet [\cos(\theta_T)]^2 + f \\ & \bullet [\cos(\theta_L)]^3 + g \bullet [\cos(\theta_T)]^3 + h \bullet \cos(\theta_L) \bullet \cos(\theta_T) + i \bullet [\cos(\theta_L)]^2 \\ & \bullet \cos(\theta_T) + j \bullet \cos(\theta_L) \bullet [\cos(\theta_T)]^2 \end{aligned} \tag{15}$$

3. Results

In the present section, the results of IAM calculations are presented. Firstly, a comparison is made between the values resulting from instantaneous ray tracing calculations and those from the well-known biaxial factored approach. Following that, the new zenith projections (ZP) correlation is considered, assessing its accuracy throughout a wide range of possible orientations of the LFC ranging from 0° to 90°. The comparison between the two approaches is carried out employing two error metrics: relative error (Δ) and root mean square error (RMSE), the latter being defined according to Eq. (16): in this equation, the variable y* represents the value derived from the approximating correlation, while y denotes the exact (reference) value, and N is the total number of observations or simulations.

$$RMSE = \sqrt{\frac{\sum_{i=1}^{N} (y_i^* - y_i)^2}{N}} \tag{16}$$

3.1. The biaxial factored approach

Initially, the FresnelSim algorithm was executed to compute the transversal and longitudinal angle modifiers, namely $IAM_{RT,T}$ and $IAM_{RT,L}$, respectively. These are essential in determining the factored angle modifier IAM_F, whose calculation was performed in accordance with Eq. (8).

As represented in Fig. 5, a comparison between the two plants reveals that the transversal component exhibits similar behaviour, while the longitudinal, more influenced by end-losses, approaches zero at lower incidence angles in the P2 plant, characterized by a shorter mirror length. Conversely, the transversal component has an irregular profile due to the combined shading effects of both the receiver assembly and adjacent mirrors. Using these calculated values, a comprehensive IAM analysis was conducted based on the factored approach. Fig. 6 demonstrates the correlation between the non-approximated instantaneous IAM_{RT} (obtained through direct ray tracing calculations) and the factored IAM_F for the NS orientation over a span of 25 days. In general, it can be inferred that the factored correlation tends to underestimate the optical performance of the system. More specifically, the root mean square error (RMSE) is found to be 0.095 in P1 and 0.108 in P2, equal to 19.42 % and 26.70 % with respect to the yearly average IAM_{RT}, while the corresponding relative errors Δ are 26.37 % and 30.53 % respectively.

In order to generalize the conclusions regarding the factored approximation accuracy, an identical methodology was employed to analyse all the possible orientations within the range of 0°–90°, with an interval of 5°. To concisely present the findings, Fig. 7 summarizes the results in terms of relative errors Δ [%] and root mean square error (RMSE) for both plant configurations. The RMSE values exhibit a slight decrease for higher orientation angles (0.090 for P1 and 0.087 for P2 at $\zeta = 90°$); however, neither the RMSE nor the relative error displays a clear dependence on orientation. Hence, it can be concluded that the factored approach, while still demonstrating low precision, does not exhibit any significant variation in accuracy with respect to plant orientation.

3.2. The transversal and longitudinal zenith angle model

The present case study starts from the approximation model proposed by the same research group, which utilizes sin(δ) and cos(θ) as independent variables within a cubic polynomial relationship: while this

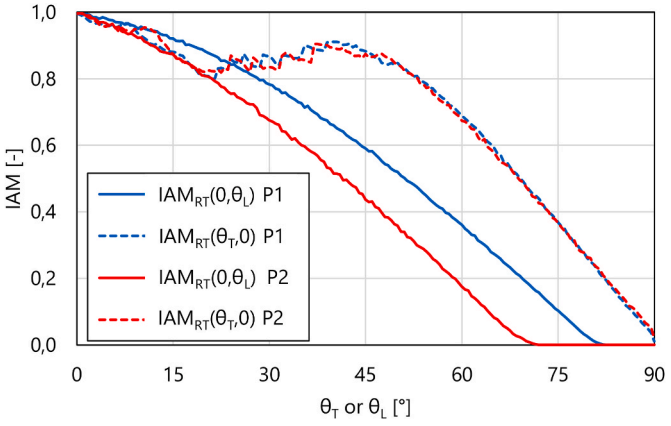

Fig. 5. Transversal and longitudinal IAM components of the two case study plants (P1 and P2).

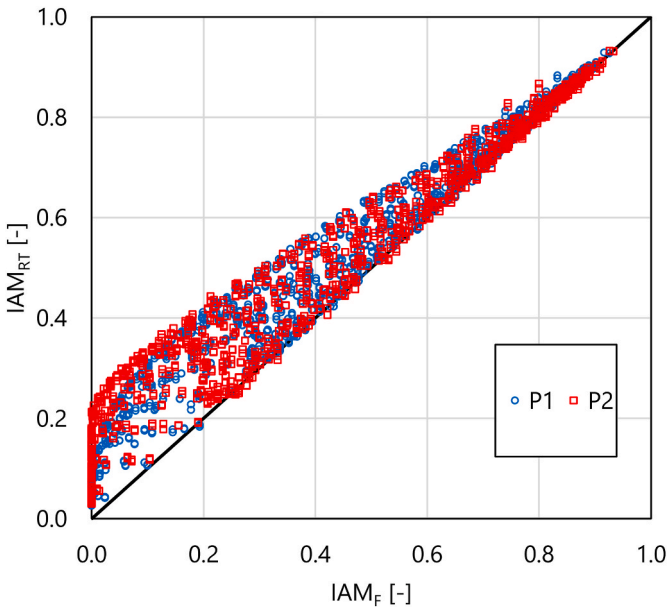

Fig. 6. Comparison between the instantaneous non-approximated IAM_{RT} and the biaxial factored approximation IAM_F, $\zeta = 0°$.

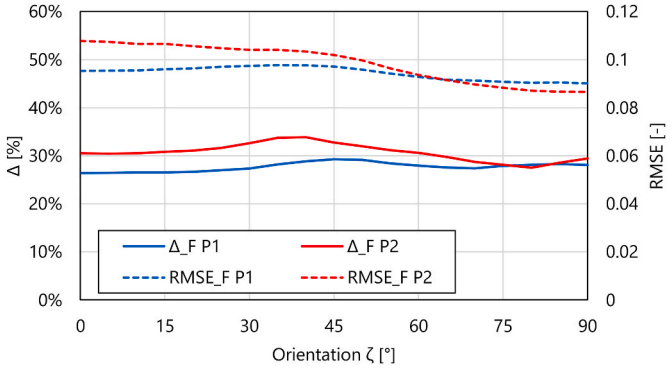

Fig. 7. Reference raytracing simulations and factored approach: RMSE and percentage error (Δ) for different plant orientations.

approach demonstrates high accuracy for standard orientations (North-South), it exhibits an increasing RMSE that surpasses the simpler factored approach when the orientation angle exceeds 45°. Therefore, it has been concluded that the applicability of this model is limited when the independent variables are sin(δ) and cos(θ); on the other hand, by substituting the aforementioned variables with the two mentioned before, namely cos (θ_L) and cos (θ_T), it has been found that the accuracy of the same polynomial model is considerably less influenced by the orientation angle.

Initially, a cubic polynomial correlation was employed, and a set of constants was determined for each orientation, resulting in an average RMSE of 0.0276 (P1) and 0.0303 (P2), corresponding to the 5.66 % and 8.18 % of the respective yearly average ray tracing values: the resulting constants, as well as the approximation errors, are reported in the following (Table 2).

The RMSE values are significantly lower than those achievable with other approximate correlations, albeit requiring the optimization of coefficients related to the specific plant orientation. In order to generalize the effectiveness of the proposed approach and reduce the computation time, a single set of coefficients was determined aimed to fit the IAM_{RT} values of all the orientations from 0° to 90°: an average RMSE of 0.030 (P1) and 0.033 (P2) was achieved (Fig. 8). The increase in RMSE compared to the calculations performed with dedicated coefficients for each orientation is almost negligible (+0.3 % for P1, 0.03 % for P2): this implies an acceptable level of accuracy in both cases that is still significantly above that provided by the factored formula. In general, it is important to note that the proposed approach demonstrates greater accuracy when applied to installations with low end losses, typically characterized by a high length-to-height (L/H) ratio, as seen in the case of P1. On the other hand, analysing individual modules with an L/H ratio closer to unity could lead to reduced accuracy.

Furthermore, considering each individual orientation separately, the robustness and accuracy of the proposed model can be assessed, even when regression coefficients are determined based on only three significant days (equinox and solstices, i.e., days number 81, 172, 355). Table 3 presents the values of these coefficients for a limited number of orientations specifically related to the P1 plant: however, it is evident that the approach is easily generalizable to other geometries. As the results demonstrate, as long as the orientation is lower than 30°, the RMSE remains substantially unchanged compared to the case where the coefficients are calculated using the complete dataset of 25 days (i.e., 0.033 for $\zeta = 0°$, 0.046 for $\zeta = 30°$), as well as the correlation coefficients R^2 (0.984 for $\zeta = 0°$, 0.975 for $\zeta = 30°$). A partial graphical representation of these results is provided in Fig. 9, where the values of instantaneous incidence angle modifiers (IAM) are shown for orientations of 0° and 30° according to this simplified approach. On the other hand, it should be noted that this simplified 3-day approach should be avoided in case of plants rotated to a large extent with respect to NS direction: the RMSE is as high as 0.119 when the system has an azimuth of 60° (R^2 equal to 0.809), and the results are even worse for EW oriented plants. This suggests that the need for a large dataset for coefficients' calibration is more stringent when the system is arranged along a non-standard direction, i.e., when its orientation angle exceeds 30°.

This observation clearly identifies the zenith projections model based on longitudinal and transverse zenith angles as a robust tool for assessing the instantaneous potential of an LFC based on its geometry and a limited database. This applies whether the database originates

Table 2
Regression constants from RMSE minimization for four significative orientations, 25-day dataset.

	$\zeta = 0°$		$\zeta = 30°$		$\zeta = 60°$		$\zeta = 90°$	
Coefficients	P1	P2	P1	P2	P1	P2	P1	P2
a	0.018	0.024	0.006	0.004	−0.004	−0.004	−0.008	−0.013
b	0.160	0.199	0.415	0.625	0.432	0.504	0.512	1.011
c	0.744	0.681	0.350	0.067	0.410	0.237	0.308	−0.107
d	−0.379	−0.289	−0.812	−1.281	−0.803	−0.631	−1.067	−0.125
e	−1.274	−1.113	−0.937	−1.092	−1.439	−1.307	−1.358	−0.252
f	0.037	−0.087	0.246	0.517	−0.227	−0.542	−0.048	−0.786
g	0.286	0.310	0.219	0.417	0.967	1.129	0.945	0.432
h	1.445	0.510	2.009	2.079	2.430	1.569	2.727	−0.416
i	0.364	1.299	0.153	0.400	1.345	2.574	1.205	2.476
j	−0.533	−0.683	−0.794	−0.897	−2.271	−2.693	−2.398	−1.370
RMSE	0.029	0.034	0.029	0.033	0.027	0.033	0.023	0.032
R^2	0.986	0.985	0.987	0.985	0.990	0.988	0.993	0.991

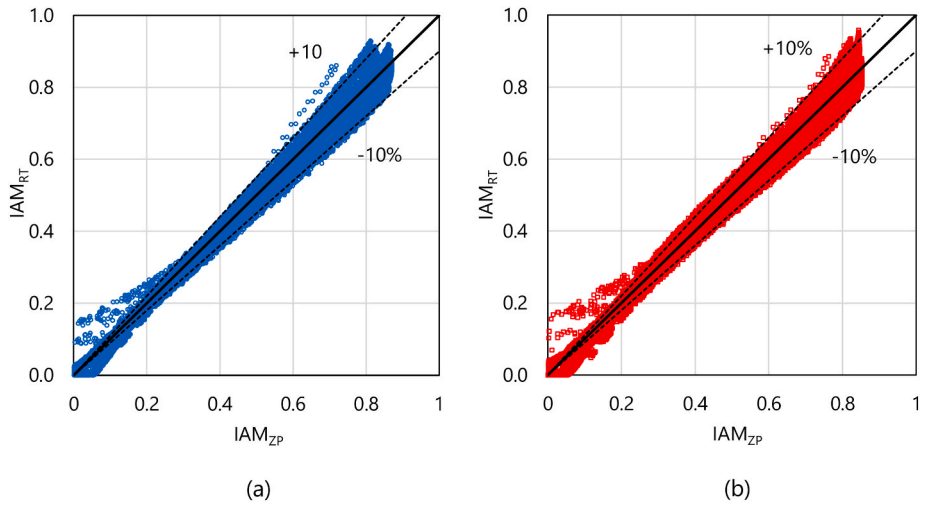

Fig. 8. Single set "zenith-projections" approximation: comparison between instantaneous non-approximated IAM_{RT} and the zenith angle projections model IAM_{ZP} based on 25 days and orientations ranging from 0° to 90° in (a) plant P1 and (b) plant P2.

Table 3
Regression constants from RMSE minimization for four significative orientations, 3-day reduced dataset, plant P1

Coefficients	ζ = 0°	ζ = 30°	ζ = 60°	ζ = 90°
A	−0.029	−0.138	−0.212	−0.050
B	0.237	0.855	0.637	0.214
C	1.014	0.956	1.791	0.890
D	−0.868	−1.538	−1.326	−0.985
E	−2.181	−2.190	−4.032	−2.526
F	0.452	0.407	0.004	0.003
G	0.833	1.089	2.491	1.546
H	2.112	1.994	2.380	3.193
I	−0.082	0.768	1.718	1.010
J	−0.616	−1.328	−2.576	−2.432
RMSE	0.033	0.045	0.119	0.173
R^2	0.984	0.975	0.809	0.657

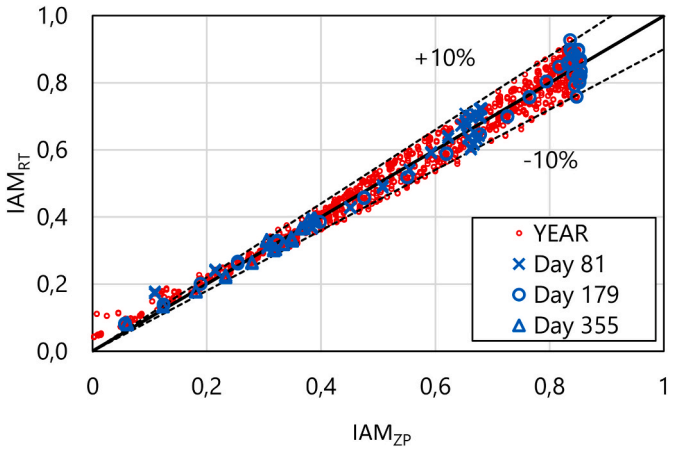

Fig. 9. Comparison between the instantaneous IAM_{RT} and the present model IAM_{ZP} for plant P1 and ζ = 0° based on the reduced 3-day dataset.

from measured real-world data or, more importantly, if the database is derived from time-consuming ray-tracing simulations.

3.3. Energy availability at the receiver aperture

In this section, the results of the previous analysis are presented in terms of energy available at the target, which is in this case represented by the flat aperture of the CPC concentrator. Specifically, the energy values resulting from ray-tracing simulations are compared with the instantaneous values derived from the factored model and the zenith projections correlation proposed in this paper. The results are again reported for three significant days of the year, namely the equinox and the two solstices, and NS-oriented P1 geometry. As can be seen in Fig. 10a, the relationship proposed by McIntire, which has been generally criticized thus far, actually proves to be quite accurate in describing the trend of available energy, particularly on summer days and especially during the central hours of the day. It is noticeable, however, that during the equinoxes and especially the winter solstice, the present model better approximates the actual trend throughout the day. Nevertheless, it is important to supplement these observations with data concerning the sum of the available energy over the entire day: by considering the ratio of daily-averaged available power from correlations to that from ray tracing, as shown in Fig. 10b, it is possible to observe that for all three days under consideration, the present relationship provides greater accuracy in describing the available energy. Specifically, while on day number 172, the factored correlation effectively describes 95 % of the energy resulting from ray tracing, albeit with lower precision compared to the newly proposed approach, it is evident that on the other days, this percentage drops significantly, indicating greater effectiveness of the relationship proposed by the authors.

The same analysis, based on the ratio of daily-averaged available power from correlations to the "exact" ray tracing values, was then extended to different orientations of the system. As depicted in Fig. 11, the zenith projections relationship maintains a similar level of accuracy even when the plant azimuth angle ζ is set to 30° or 60° throughout the year. On the other hand, the factored approach is characterized not only by lower accuracy but also by a certain sensitivity to the orientation angle itself: this is particularly evident in summer when the results worsen with increasing orientation angle, and in winter when the accuracy achievable with the factored approach is directly proportional to the deviation from the north-south direction.

4. Conclusions

This research has been aimed at proposing a new correlation to calculate the Incidence Angle Modifier (IAM) of Linear Fresnel Collectors (LFCs) based on transversal and longitudinal projections of the zenith angle, namely θ_T, and θ_L. This new approach, devoted to instantaneous opto-energy analysis, is intended to be more accurate with respect to the well-established factored formulation by McIntire; on the other hand, it has the advantage of requiring reduced computation time

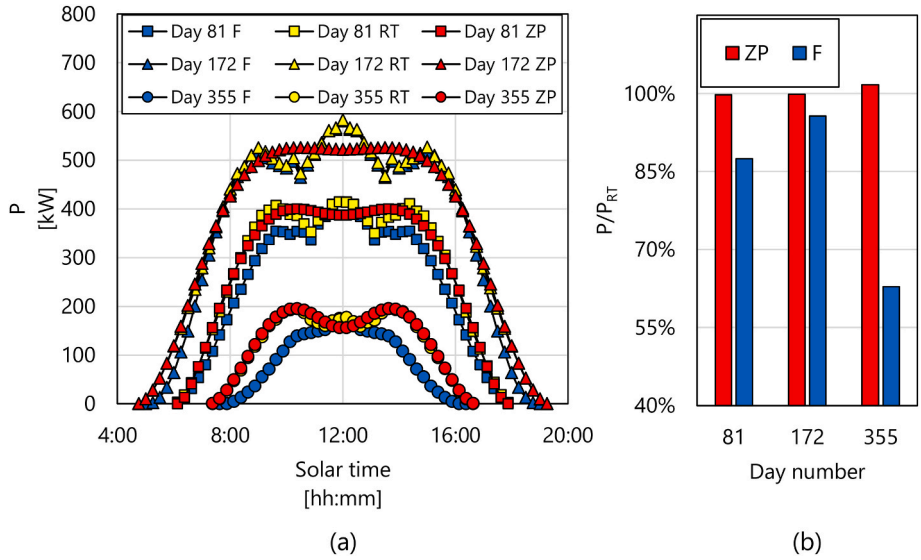

Fig. 10. Available power (P) at the P1 CPC aperture, $\zeta = 0°$: (a) instantaneous values from ray tracing (RT), factored (F) and zenith projections (ZP) correlations and (b) ratio of daily-averaged available power by correlations (P) to ray tracing values (P_{RT}).

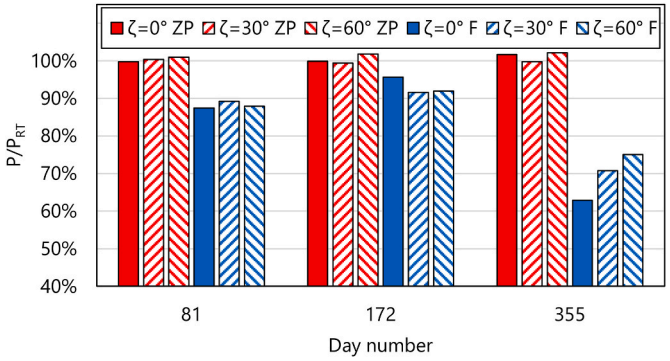

Fig. 11. Ratio of daily-averaged available power by correlations (P) to ray tracing values (P_{RT}) at different system orientations.

compared to full ray-tracing analyses. The proposed correlation is in the form of a zenith projections regression model whose constants have been herein determined based on reference IAM data obtained by verified ray tracing calculations: collectors' dimensions and properties have been taken from two real plants (here named P1 and P2) located, respectively, in Partanna (Italy) and Ben Guerir (Morocco). For comparison purposes, the IAM has been calculated for a large set of possible orientation angles from 0° to 90° according to the factored approach, resulting in an average Root Mean Square Error (RMSE) equal to 0.094 (P1) and 0.098 (P2). The main limitation of the correlation presented by McIntire (which still remains very compact as a concept and as a formula) lies in the fact that it factorizes phenomena that are not factorable. The IAM has then been determined based on the proposed zenith projections approach: sub-hourly results are considered against the exact ray tracing values obtained for both plants over 25 days. The RMSE, averaged over all the considered orientations, decreased to 0.030 (P1) when the regression coefficients are determined at each plant arrangement: on the other hand, it has been demonstrated that a single set of coefficients is able to fit the real IAM values as well, resulting in a substantially unchanged RMSE. Another important finding is related to the robustness of the present incidence angle model, especially in applications characterized by alignments in the range of 0°–30° with respect to NS direction: it has in fact been found that a high level of accuracy is obtainable even when a reduced raytracing dataset of 3 days is used to calculate the regression constant, thus further reducing the needed computation time.

Finally, three reference days are considered to examine the power availability at the secondary reflector according to the two mentioned correlations: it has been found that the factored approach provides very precise outputs in the hours around noon during summer but, at the same time, always underperforms the daily average 3rd order polynomial results.

CRediT authorship contribution statement

Samuele Memme: Formal analysis, Software, Validation, Visualization, Writing – original draft, Writing – review & editing. **Marco Fossa:** Conceptualization, Investigation, Methodology, Supervision, Writing – review & editing.

Declaration of competing interest

The authors declare that they have no known competing financial interests or personal relationships that could have appeared to influence the work reported in this paper.

Acknowledgments

ENEA research center, Solar Thermal Division, is acknowledged for the useful discussions provided about the Partanna Fresnel Plan.

The Authors acknowledge Dr. Alessia Boccalatte for her contributions to develop parts of the FresnelSim code.

References

[1] IRENA, Renewable Capacity Statistics 2022, 2022. Abu Dhabi, https://www.irena.org/publications/2022/Apr/Renewable-Capacity-Statistics-2022. (Accessed 22 May 2023).
[2] IEA, in: Renewables 2022, Paris, 2022. https://www.iea.org/reports/renewables-2022. (Accessed 22 May 2023).
[3] C. Hernández Moris, M.T. Cerda Guevara, A. Salmon, A. Lorca, Comparison between concentrated solar power and gas-based generation in terms of economic and flexibility-related aspects in Chile, Energies 14 (2021) 1063, https://doi.org/10.3390/en14041063.
[4] IRENA, Renewable Power Generation Costs in 2021, 2022. Abu Dhabi, https://www.irena.org/publications/2022/Jul/Renewable-Power-Generation-Costs-in-2021. (Accessed 21 February 2023).
[5] M.M. Njore, J.E. Sinton, Concentrating Solar Power: Clean Power on Demand, 24/7, 2021. Washington, https://pubdocs.worldbank.org/en/849341611761898393/WorldBank-CSP-Report-Concentrating-Solar-Power-Clean-Power-on-Demand-24-7-FINAL. (Accessed 1 February 2023).

[6] H. Al-Kayiem, S. Mohammad, Potential of renewable energy resources with an emphasis on solar power in Iraq: an outlook, Resources 8 (2019) 42, https://doi.org/10.3390/resources8010042.
[7] P. Kurup, C. Turchi, Initial Investigation into the Potential of CSP Industrial Process Heat for the Southwest United States, CO, Golden, 2015.
[8] A. Häberle, D. Krüger, Concentrating solar technologies for industrial process heat, in: Concentrating Solar Power Technology, Elsevier, 2021, pp. 659–675, https://doi.org/10.1016/B978-0-12-819970-1.00011-6.
[9] E. Bellos, D. Korres, C. Tzivanidis, K.A. Antonopoulos, Design, simulation and optimization of a compound parabolic collector, Sustain. Energy Technol. Assessments 16 (2016) 53–63, https://doi.org/10.1016/j.seta.2016.04.005.
[10] A. Rabl, Optical and thermal properties of compound parabolic concentrators, Sol. Energy 18 (1976) 497–511, https://doi.org/10.1016/0038-092X(76)90069-4.
[11] G. Zhu, Development of an analytical optical method for linear Fresnel collectors, Sol. Energy 94 (2013) 240–252, https://doi.org/10.1016/j.solener.2013.05.003.
[12] H.H. Sait, J.M. Martinez-Val, R. Abbas, J. Munoz-Anton, Fresnel-based modular solar fields for performance/cost optimization in solar thermal power plants: a comparison with parabolic trough collectors, Appl. Energy 141 (2015) 175–189, https://doi.org/10.1016/j.apenergy.2014.11.074.
[13] G. Morin, J. Dersch, W. Platzer, M. Eck, A. Häberle, Comparison of linear Fresnel and Parabolic Trough collector power plants, Sol. Energy 86 (2012) 1–12, https://doi.org/10.1016/j.solener.2011.06.020.
[14] R. Abbas, J. Muñoz, J.M. Martínez-Val, Steady-state thermal analysis of an innovative receiver for linear Fresnel reflectors, Appl. Energy 92 (2012) 503–515, https://doi.org/10.1016/J.APENERGY.2011.11.070.
[15] R. Abbas, M.J. Montes, A. Rovira, J.M. Martínez-Val, Parabolic trough collector or linear Fresnel collector? A comparison of optical features including thermal quality based on commercial solutions, Sol. Energy 124 (2016) 198–215, https://doi.org/10.1016/j.solener.2015.11.039.
[16] N. Kincaid, G. Mungas, N. Kramer, M. Wagner, G. Zhu, An optical performance comparison of three concentrating solar power collector designs in linear Fresnel, parabolic trough, and central receiver, Appl. Energy 231 (2018) 1109–1121, https://doi.org/10.1016/j.apenergy.2018.09.153.
[17] H. Schenk, T. Hirsch, J. Fabian Feldhoff, M. Wittmann, Energetic comparison of linear Fresnel and Parabolic Trough collector systems, J. Sol. Energy Eng. 136 (2014), https://doi.org/10.1115/1.4027766.
[18] G. Cau, D. Cocco, Comparison of medium-size concentrating solar power plants based on Parabolic Trough and linear Fresnel collectors, Energy Proc. 45 (2014) 101–110, https://doi.org/10.1016/j.egypro.2014.01.012.
[19] A. Boccalatte, M. Fossa, C. Ménézo, Calculation of the incidence angle modifier of a Linear Fresnel Collector: the proposed declination and zenith angle model compared to the biaxial factored approach, Renew. Energy 185 (2022) 123–138, https://doi.org/10.1016/j.renene.2021.12.017.
[20] G. Wang, F. Wang, F. Shen, T. Jiang, Z. Chen, P. Hu, Experimental and optical performances of a solar CPV device using a linear Fresnel reflector concentrator, Renew. Energy 146 (2020) 2351–2361, https://doi.org/10.1016/j.renene.2019.08.090.
[21] G. Wang, F. Shen, F. Wang, Z. Chen, Design and experimental study of a solar CPV system using CLFR concentrator, Sustain. Energy Technol. Assessments 40 (2020), 100751, https://doi.org/10.1016/j.seta.2020.100751.
[22] R. Abbas, J.M. Martínez-Val, Analytic optical design of linear Fresnel collectors with variable widths and shifts of mirrors, Renew. Energy 75 (2015) 81–92, https://doi.org/10.1016/J.RENENE.2014.09.029.
[23] P.L. Singh, S. Ganesan, G.C. Yàdav, Performance study of a linear Fresnel concentrating solar device, Renew. Energy 18 (1999) 409–416, https://doi.org/10.1016/S0960-1481(98)00805-2.
[24] A. Heimsath, G. Bern, D. van Rooyen, P. Nitz, Quantifying optical loss factors of small linear concentrating collectors for process heat application, Energy Proc. 48 (2014) 77–86, https://doi.org/10.1016/j.egypro.2014.02.010.
[25] P. Boito, R. Grena, Optimal focal length of primary mirrors in Fresnel linear collectors, Sol. Energy 155 (2017) 1313–1318, https://doi.org/10.1016/j.solener.2017.07.079.
[26] P. Shaoxuan, X. Chaofeng, End-effect of linear Fresnel collectors, in: 2011 Asia-Pacific Power and Energy Engineering Conference, IEEE, 2011, pp. 1–4, https://doi.org/10.1109/APPEEC.2011.5748793.
[27] S. Benyakhlef, A. Al Mers, O. Merroun, A. Bouatem, N. Boutammachte, S. El Alj, H. Ajdad, Z. Erregueragui, E. Zemmouri, Impact of heliostat curvature on optical performance of Linear Fresnel solar concentrators, Renew. Energy 89 (2016) 463–474, https://doi.org/10.1016/j.renene.2015.12.018.
[28] S. Memme, M. Fossa, Maximum energy yield of PV surfaces in France and Italy from climate based equations for optimum tilt at different azimuth angles, Renew. Energy 200 (2022) 845–866, https://doi.org/10.1016/j.renene.2022.10.019.
[29] G. Barale, A. Heimsath, P. Nitz, A. Toro, Optical design of a linear Fresnel collector for sicily, SolarPaces Conf (2010) 1–7.
[30] D. Feuermann, J.M. Gordon, Analysis of a two-stage linear Fresnel reflector solar concentrator, J. Sol. Energy Eng. 113 (1991) 272–279, https://doi.org/10.1115/1.2929973.
[31] R. Abbas, J. Muñoz-Antón, M. Valdés, J.M. Martínez-Val, High concentration linear Fresnel reflectors, Energy Convers. Manag. 72 (2013) 60–68, https://doi.org/10.1016/j.enconman.2013.01.039.
[32] R. Abbas, M. Valdés, M.J. Montes, J.M. Martínez-Val, Design of an innovative linear Fresnel collector by means of optical performance optimization: a comparison with parabolic trough collectors for different latitudes, Sol. Energy 153 (2017) 459–470, https://doi.org/10.1016/j.solener.2017.05.047.
[33] F. Huang, L. Li, W. Huang, Optical performance of an azimuth tracking linear Fresnel solar concentrator, Sol. Energy 108 (2014) 1–12, https://doi.org/10.1016/j.solener.2014.06.028.
[34] V. Sharma, J.K. Nayak, S.B. Kedare, Effects of shading and blocking in linear Fresnel reflector field, Sol. Energy 113 (2015) 114–138, https://doi.org/10.1016/j.solener.2014.12.026.
[35] E. Montanet, S. Rodat, Q. Falcoz, F. Roget, Influence of topography on the optical performances of a Fresnel linear asymmetrical concentrator array: the case of the eLLO solar power plant, Energy 274 (2023), 127310, https://doi.org/10.1016/j.energy.2023.127310.
[36] S. Karathanasis, Linear Fresnel Reflector Systems for Solar Radiation Concentration, 2019, https://doi.org/10.1007/978-3-030-05279-9.
[37] J.D. Hertel, V. Martinez-Moll, R. Pujol-Nadal, Estimation of the influence of different incidence angle modifier models on the biaxial factorization approach, Energy Convers. Manag. 106 (2015) 249–259, https://doi.org/10.1016/j.enconman.2015.08.082.
[38] K. Lovegrove, W. Stein, Concentrating Solar Power Technology, Woodhead Publishing Limited, 2012, https://doi.org/10.1533/9780857096173.
[39] W.R. McIntire, Factored approximations for biaxial incident angle modifiers, Sol. Energy 29 (1982) 315–322, https://doi.org/10.1016/0038-092X(82)90246-8.
[40] M. Fossa, A. Boccalatte, S. Memme, Solar Fresnel modelling, geometry enhancement and 3D ray tracing analysis devoted to different energy efficiency definitions and applied to a real facility, Sol. Energy 216 (2021) 75–89, https://doi.org/10.1016/j.solener.2020.12.047.
[41] S. Memme, M. Fossa, Ray tracing analysis of linear Fresnel concentrators and the effect of plant azimuth on their optical efficiency, Renew. Energy 216 (2023), 119121, https://doi.org/10.1016/j.renene.2023.119121.
[42] M.J. Blanco, J.M. Amieva, A. Mancillas, The Tonatiuh Software Development Project: an open source approach to the simulation of solar concentrating systems, in: ASME 2005 International Mechanical Engineering Congress and Exposition, American Society of Mechanical Engineers, 2005, pp. 157–164.
[43] T. Wendelin, SolTRACE: a new optical modeling tool for concentrating solar optics, in: Proceedings of the ISEC 2003: International Solar Energy Conference, American Society of Mechanical Engineers, Kohala Coast, New York, 2003, pp. 253–260. Hawaii.
[44] M. Izygon, P. Armstrong, C. Nilsson, N. Vu, A GPU-based suite of software for central receiver solar power plants, in: Proceedings of SolarPACES, 2011.
[45] G. Cardona, R. Pujol-Nadal, OTSun, a python package for the optical analysis of solar-thermal collectors and photovoltaic cells with arbitrary geometry, PLoS One 15 (2020), e0240735, https://doi.org/10.1371/journal.pone.0240735.
[46] TracePro Lambda. https://lambdares.com/tracepro, 2019. (Accessed 22 February 2023).
[47] D. Gebreiter, G. Weinrebe, M. Wöhrbach, F. Arbes, F. Gross, W. Landman, sbpRAY – A Fast and Versatile Tool for the Simulation of Large Scale CSP Plants, 2019, 170004, https://doi.org/10.1063/1.5117674.
[48] J.A. Duffie, W.A. Beckman, Solar Engineering of Thermal Processes, John Wiley & Sons, Inc., Hoboken, NJ, USA, 2013, https://doi.org/10.1002/9781118671603.
[49] A. Giostri, M. Binotti, P. Silva, E. Macchi, G. Manzolini, Comparison of two linear collectors in solar thermal plants: parabolic Trough versus Fresnel, J. Sol. Energy Eng. 135 (2013), https://doi.org/10.1115/1.4006792.
[50] R. Pujol Nadal, V. Martínez Moll, Optical analysis of the fixed mirror solar concentrator by forward ray-tracing procedure, Journal of Solar Energy Engineering, Transactions of the ASME 134 (2012), https://doi.org/10.1115/1.4006575.
[51] Frenell GmbH, Frenell website, (n.d.). https://www.frenell.de/it/(accessedMarch 3, 2023) .
[52] National Renewable Energy Laboratory (NREL), Partanna MS-LFR CSP Project, (n.d.). https://solarpaces.nrel.gov/project/partanna-ms-lfr (accessedMarch 3, 2023) .
[53] M. Falchetta, D. Mazzei, V. Russo, V.A. Campanella, V. Floridia, B. Schiavo, L. Venezia, C. Brunatto, R. Orlando, The Partanna Project: A First of a Kind Plant Based on Molten Salts in LFR Collectors, 2020, 040001, https://doi.org/10.1063/5.0029269.
[54] FATA - Part of Danieli Group, SOLINPAR CSP plant in Partanna – Sicily – Entered into Production, (n.d.). https://www.fatagroup.it/solinpar-csp-plant-in-partanna-sicily-entered-into-production/(accessed March 3, 2023) .
[55] (n.d. Green Energy Park. https://www.greenenergypark.ma/. (Accessed 23 May 2023).
[56] I. Ortega-Fernández, A.B. Hernández, Y. Wang, D. Bielsa, Performance assessment of an oil-based packed bed thermal energy storage unit in a demonstration concentrated solar power plant, Energy 217 (2021), 119378, https://doi.org/10.1016/j.energy.2020.119378.
[57] Delco Company, Delcoterm solar E15 data sheet, (n.d.). http://delcosrl.com/en/prodotti_2.aspx (accessed May 18, 2023) .
[58] Microsoft® BingTM Maps, Map showing the Partanna Fresnel plant 37.70° N, 12.86° E [Online] Available at: http://it.bing.com/maps/ (accessed March 3, 2023).
[59] Google Earth 7.3. Map showing the Partanna Fresnel plant 37.70° N, 12.86° E, 2023 [Online] Available at: http://www.google.com/earth/index.html (accessed March 3, 2023).

[60] J. Cumpston, J. Coventry, Derivation of Error Sources for Experimentally Derived Heliostat Shapes, 2017, 030013, https://doi.org/10.1063/1.4984356.
[61] R. Abbas, A. Sebastián, M.J. Montes, M. Valdés, Optical features of linear Fresnel collectors with different secondary reflector technologies, Appl. Energy 232 (2018) 386–397, https://doi.org/10.1016/j.apenergy.2018.09.224.
[62] P. Tsekouras, C. Tzivanidis, K. Antonopoulos, Optical and thermal investigation of a linear Fresnel collector with trapezoidal cavity receiver, Appl. Therm. Eng. 135 (2018) 379–388, https://doi.org/10.1016/j.applthermaleng.2018.02.082.